

# Transport limited effects in a model of dendritic branching

Bruce P. Graham<sup>a,\*</sup>, Arjen van Ooyen<sup>b,1</sup>

<sup>a</sup>*Department of Computing Science and Mathematics, University of Stirling, Stirling FK9 4LA, UK*

<sup>b</sup>*Netherlands Institute for Brain Research, Meibergdreef 33, 1105 AZ Amsterdam, The Netherlands*

Received 17 December 2003; received in revised form 7 June 2004; accepted 11 June 2004

Available online 30 July 2004

## Abstract

A variety of stochastic models of dendritic growth in developing neurons have been formulated previously. Such models indicate that the probability of a new branch forming in a growing tree may be modulated by factors such as the number of terminals in the tree and their centrifugal order. However, these models cannot identify any underlying biophysical mechanisms that may cause such dependencies. Here, we explore a new model in which branching depends on the concentration of a branch-determining substance in each terminal segment. The substance is produced in the cell body and is transported by active transport and diffusion to the terminals. The model reveals that transport-limited effects may give rise to the same modulation of branching as indicated by the stochastic models. Different limitations arise if transport is dominated by active transport or by diffusion.

© 2004 Elsevier Ltd. All rights reserved.

**Keywords:** Dendritic branching; ODE model; Active transport; Diffusion; Tubulin

## 1. Introduction

One of the major distinguishing features of neurons is their morphology. Thin branches (neurites) extending from the cell body form the sites of input and output from a neuron. The branches known as dendrites are the major sites of input and form trees with topologically and geometrically characteristic branching patterns for different neuronal types. Dendritic trees can be classified according to the number of terminals, the symmetry of the tree, and the lengths, diameters and branching angles of intermediate segments between branch points and terminal segments (Hillman, 1979; van Pelt and Uylings, 1999).

Dendritic morphology arises during development from the elongation and branching of neurites. Growth cones at the tips of developing neurites determine the direction of neurite extension and if and when a neurite branches. Rates of elongation and branching are determined both by the external environment and by the internal state of the neurite. Whether or not a branching event occurs is influenced by the state of the actin and microtubule cytoskeletons. Branching firstly involves the splitting of the growth cone, including a rearrangement of its actin cytoskeleton. The new branches are eventually stabilized by the formation of rigid microtubule bundles in the trailing neurite and into the growth cones. Rho proteins regulate rearrangement of the actin cytoskeleton in response to internal and external signals (Acebes and Ferrus, 2000; Redmond and Ghosh, 2001; Whitford et al., 2002). The stability of microtubule bundles is regulated by microtubule-associated proteins (MAPs) (Maccioni and Cambiazo, 1995; Kobayashi and Mundel, 1998). Phosphorylation of MAPs destabilizes the microtubule bundles and has been correlated with increased neurite branching

\*Corresponding author. Tel.: +44-1786-467432; fax: +44-1786-464551.

E-mail address: [b.graham@cs.stir.ac.uk](mailto:b.graham@cs.stir.ac.uk) (B.P. Graham).

<sup>1</sup>Present address: Department of Experimental Neurophysiology, Center for Neurogenomics and Cognitive Research (CNCR), Vrije Universiteit, De Boelelaan 1085 1081 HV Amsterdam, The Netherlands.

(Audesirk et al., 1997). Many other factors also influence neurite outgrowth and branching, including calcium entry through membrane-bound ion channels and synaptic and intrinsic electrical activity (Cline, 2001).

Remarkably, simple models of dendritic growth that describe elongation and branching as stochastic processes are sufficient to generate the topological and metrical features from a wide range of neuronal tree types (van Pelt et al., 1997; van Pelt and Uylings, 1999; Dityatev et al., 1995; Uemura et al., 1995; Nowakowski et al., 1992; Carriquiry et al., 1991). As described above, the actual dendritic growth process is highly complex, leading to the apparently stochastic nature of elongation and branching (van Pelt and Uylings, 1999). These statistical models of tree growth do not directly identify the underlying biophysical processes involved in dendritic development. As a consequence they give little insight into how a neuron's intracellular environment and its interaction with other neurons and the extracellular space influences its morphological development. The particular biophysical differences in growth between different neuronal types are not identified. New models that incorporate biophysically identifiable parameters and processes are needed to address these issues.

To develop such models, we use as a starting point the statistical models that describe dendritic tree development as a stochastic growth process in time. The most parsimonious of these is the *BESTL* model of van Pelt and coworkers (van Pelt et al., 1997; van Pelt and Uylings, 1999). Their model contains a small number of parameters that can be tuned to reproduce certain characteristics of the trees from a large number of neuronal types. In particular, the model reproduces the branching structure of a dendritic tree, which is described in terms of the number of terminal segments (degree) and their centrifugal order (the number of branch points between the terminal and the root of the tree). It does not seek to reproduce dendritic growth in 3D space. Nonetheless, the statistics of degree and centrifugal order distributions is sufficient to distinguish the trees of different neuronal types. Intriguingly, this model indicates that the branching process that generates the dendritic tree is modulated by the total number of terminals in the growing tree and their centrifugal order. It is an open question as to the biophysical processes that may produce these dependencies.

Here we introduce a new model that indicates such dependencies may arise from intracellular transport-limited effects if branching in part depends on a substance that is produced in the cell body and is transported by active transport and diffusion to the tree terminals. Branching is influenced by the ability of the internal cytoskeleton to be remodelled to form new neurite branches. Limiting factors here include the

availability of cytoskeletal proteins, such as tubulin, and the stability of the existing cytoskeleton. Consequently, possible candidates for the role of “branch determining substance” include tubulin and microtubule-associated proteins (MAPs). Tubulin is required at neurite tips for the assembly of microtubules, resulting in neurite elongation and the possible formation of new branches. Microtubule construction and stability are influenced by MAPs. Dendritic branching has been correlated with the phosphorylation state of MAP2 (Audesirk et al., 1997). Other branch determining substances include factors that effect the stability of the actin network in the growth cone, such as Rho proteins. Whichever the actual substance, we investigate here how the interactions between production, transport and consumption of such a substance affect the branching process. The model assumes that the synthesis of the branch determining substance takes place in the cell body. This is likely the case at least during the initial stages of neurite development, although local protein synthesis may occur in adult neurites (Alvarez et al., 2000). The model is also relevant to outgrowth from a point of synthesis that may be located in a dendrite, but remote from the growth cones.

## 2. Models of dendritic growth over time

As with the *BESTL* model (van Pelt and Uylings, 1999), our new model describes dendritic growth as a stochastic process in which each terminal segment in the growing tree has a probability of branching to form two new daughter segments in any given short time period. The major difference is that we have a model that is formulated using biophysical processes, and we investigate the conditions in our model that give a similar effective modulation of the branching probability over time as in the *BESTL* model. Both models are concerned only with the topological structure of a dendritic tree and not its shape in 3D space. Segment length distributions are generated in the *BESTL* model by appropriate selection of terminal segment elongation rates. Our model uses the same strategy for implementing elongation. The important difference between the models is in how branching events are created. Before introducing the new model, we give a brief overview of the *BESTL* model, against which it will be compared.

### 2.1. The *BESTL* model

The *BESTL* model (van Pelt and Uylings, 1999) describes the probability,  $p_i$ , that terminal segment  $i$  will branch to form two daughter terminal segments by the equation:

$$p_i = C2^{-S_i}n^{-E}(B/N), \quad (1)$$

where  $B/N$  is a fixed probability factor for branching in any one of the  $N$  time bins of the growth period;  $n$  is the total number of terminals in the tree at the current time bin and  $E$  is the factor by which  $n$  affects the branching probability;  $\gamma_i$  is the centrifugal order of the terminal segment (number of branch points currently between the terminal segment and the cell body) and  $S$  is the factor by which  $\gamma_i$  affects the branching probability;  $C = n / \sum_{j=1}^n 2^{-S\gamma_j}$  is a normalisation factor over the dependency on centrifugal order.

Implementation of the model in a computer simulation requires dividing the growth period into a number of short time bins,  $N$  (see, van Pelt and Uylings (1999, 2002) for details of how real time might be mapped to simulated time to account for the base branching rate  $B$  varying over time). For a given time bin, each terminal segment may branch with a probability given by Eq. (1). When a branching event occurs, two daughter terminal segments of initially short length are added to the old terminal segment. Each new terminal segment is assigned a fixed elongation rate drawn from a probability distribution. All terminal segments are elongated an amount for the time bin according to their rates.

The degree and centrifugal order distributions of the dendritic trees of many different neuronal types can be matched with this model by suitable choice of the parameter values (van Pelt and Uylings, 1999; van Pelt et al., 1997, 2001, 2003). Values of  $E$  are consistently positive, indicating a decline in branching probability as the number of terminals in the tree increases. This can be interpreted as an effect of growth cones competing for some limited resource (van Pelt et al., 2003). Some tree types require a positive value for  $S$  as well, indicating a further decline in branching probability with a terminal's centrifugal order. Purkinje cell data is matched with a negative  $S$  value (van Pelt et al., 2001), corresponding to an apparent increase in branching probability with centrifugal order. These differing  $S$  values could be interpreted as larger subtrees being either more ( $S < 0$ ) or less ( $S > 0$ ) successful than smaller subtrees in competing for a limited resource that modulates the branching probability of growth cones. In spite of these interpretations, it is difficult to relate the parameters of this model directly with biophysical processes. In particular, the normalisation constant,  $C$ , implies each terminal has some global knowledge about every other terminal in the tree.

## 2.2. The active transport—diffusion (AD) model

In our new model, a substance is transported by a combination of active transport and diffusion from its site of production in the cell body to the terminal segments. Branching is a function of the amount of this substance available in each terminal of the growing tree. The spatial production, consumption, decay and trans-

port of this branch-determining substance results in a branching process which also shows dependency both upon the number of terminals in the growing tree and upon their centrifugal order.

In this model, the branch-determining substance has concentration  $C_T$  in terminal segment  $T$  in the growing tree. The branching probability of terminal segment  $T$  during a short time period  $dt$  is given by  $p_T = k_b C_T dt$ . The fixed branching rate,  $k_b$  and the time interval  $dt$  are chosen so that  $p_T < 1$ . A branch event results in a bifurcation of the terminal segment. The substance is produced at rate  $I$  in the cell body (location 0: root of the tree) and decays there at rate  $\gamma_0$ . The substance also decays (or is consumed by the branching process) at rate  $\gamma_T$  in terminal  $T$ . The substance is transported between its site of production and the tree terminals with active transport rate,  $a$  and diffusion coefficient,  $D$ . Terminal segments elongate at a fixed rate, so the terminals are constantly moving further from the cell body. The changes in concentration over time in the cell body (location 0), an intermediate segment (location  $i$  with daughter branches  $l$  and  $r$ ), and in a terminal segment (location  $T$ ) are given by

$$\frac{dC_0}{dt} = I - \gamma_0 C_0 - \frac{aA_1}{V_0} C_0 - \frac{DA_1}{L_1 V_0} (C_0 - C_1), \quad (2)$$

$$\begin{aligned} \frac{dC_i}{dt} = & \frac{aA_i}{V_i} C_{i-1} - \frac{a(A_l + A_r)}{V_i} C_i + \frac{DA_i}{L_i V_i} (C_{i-1} - C_i) \\ & - \frac{DA_l}{L_l V_i} (C_i - C_l) - \frac{DA_r}{L_r V_i} (C_i - C_r), \end{aligned} \quad (3)$$

$$\frac{dC_T}{dt} = -\gamma_T C_T + \frac{aA_T}{V_T} C_i + \frac{DA_T}{L_T V_T} (C_i - C_T), \quad (4)$$

where  $L_i$  is the length of an unbranched segment and  $A_i$  is its cross-sectional area (assumed uniform along its length). All concentrations are measured in a small volume  $V_i = A_i \Delta L$  at the distal end of a segment (small length  $\Delta L = 1 \mu\text{m}$  in the results to follow).

The model is implemented numerically by taking the first order Euler finite difference approximations for the differential equations. At each time step the concentrations,  $C_i$ , at the distal ends of every segment (terminal and intermediate) in the tree and  $C_0$  in the cell body, are calculated. Also at each time step every terminal segment is examined for a branching event, with the probability of branching,  $p_T$ , within time interval  $dt$  being as given above. When a branching event takes place, two short daughter terminal segments are instantaneously added to the end of the existing terminal segment (van Pelt et al., 2001), which then becomes an intermediate segment. Following a branching event, all segment diameters in the tree are updated according to the scheme 0 below. Note that terminal segment diameters do not change. The cell body remains the same size throughout.

Transport rates are a function of cross-sectional area in this model. Consequently, how segment diameters develop over time is important. The physical diameters of many adult dendrites approximately follow a power law (Hillman, 1979; van Pelt and Uylings, 1999):

$$d_p^e = d_l^e + d_r^e, \quad (5)$$

where  $d_p$  is the diameter of the parent segment to two (left and right) daughter segments,  $d_l$  and  $d_r$ . Particular tree types display branch powers in the range  $1 \leq e \leq 3$  (Hillman, 1979; van Pelt and Uylings, 1999). A value of  $e = 1.5$  provides electrical impedance matching through a branch point (Rall, 1959). A branch power of  $e = 2$  conserves the total cross-sectional area through a branch point. Segment diameters become increasingly uniform throughout the tree at high values of  $e$ . Adult trees corresponding to this observed range of  $e$  values have a relatively large root diameter, with diameters decreasing as the tree is traversed to the terminal segments. Intermediate segments may, or may not display significant tapering (Burke et al., 1992; Hillman, 1979). Terminal segments are relatively uniform in diameter for a given tree (Hillman, 1979). Parent segments of relatively more highly branched subtrees have larger diameters than their siblings.

It is likely that as a tree grows, segment diameters increase gradually over time to finally reach their adult size. We use an approximation to such a continuous increase in segment diameters. Segment diameters are adjusted instantaneously following each new branching event so that all segments in the tree satisfy the branch power law given above for the specified value of  $e$ . Each new terminal segment takes a small, constant diameter,  $d_T$ . The diameters of all proximal segments are increased to match the power law at each branch point.

In the results to follow we explore a wide range of branch powers, including values outside the range determined from the diameters of real neurites. We do this because the cross-sectional areas that result provide the effective transport area, but do not necessarily have to correspond to the anatomical cross-sectional area. It is possible that the cross-sectional area devoted to active transport is not a linear function of segment diameter. Microtubules provide the support for active transport. Microtubule number is correlated with neurite diameter, but microtubule density decreases with diameter (Alvarez et al., 2000), in accord with the above argument. The area available to free diffusion of molecules may also not be a simple linear function of segment diameter.

### 2.3. AD model parameter values

The transport of cytoskeletal proteins along growing neurites is thought to be predominantly by slow active transport (Galbraith et al., 1999; Kobayashi and Mundel, 1998; Miller and Samuels, 1997; Shah and

Cleveland, 2002). In most of the simulations that follow we therefore take the diffusion rate  $D = 0$ . The slow transport rate of different proteins is reasonably conserved. For example, the slow transport rate for oligomeric tubulin in the squid giant axon has been measured at about  $100 \mu\text{m}/\text{h}$  (Galbraith et al., 1999), whereas polymerized neurofilaments are transported at around  $50 \mu\text{m}/\text{h}$  (Galbraith et al., 1999). However, diffusion may also contribute to the transport. Diffusion rates vary greatly with the medium and the size of the diffusing molecule. The diffusion rate of tubulin within the squid giant axon is around  $30,000 \mu\text{m}^2/\text{h}$  (Galbraith et al., 1999). Tubulin diffuses at around  $150,000 \mu\text{m}^2/\text{h}$  in buffer, while neurofilaments diffuse at around  $1500 \mu\text{m}^2/\text{h}$  in axoplasm (Galbraith et al., 1999). The axoplasmic values for oligomeric tubulin will be used as the basic transport rates for our branch determining substance. However, we explore the effects of a wide range of parameter values, including transport rates, so our results are not restricted to tubulin as a branch determining substance.

Tubulin concentrations are in the micromolar range (Mitchison and Kirschner, 1984; Odde, 1997). The production  $I$ , somatic decay  $\gamma_0$ , and terminal consumption and decay  $\gamma_T$  rates are chosen to give an initial concentration of  $1 \mu\text{M}$  in the soma and neurite.  $\gamma_T$  may be equated with the assembly rate of free tubulin into microtubules in a terminal segment. On the basis of microtubule density in squid giant axon (Alvarez et al., 2000) and the number of tubulin subunits in  $1 \mu\text{m}$  of a microtubule (Odde, 1997), consumption of free tubulin is on the order of  $1 \mu\text{M}/\text{h}$  for elongation rates of around  $1 \mu\text{m}/\text{h}$ . For most of the results that follow we take  $\gamma_T = 100/\text{h}$ . Conditions ranging from high ( $I = 1000 \mu\text{M}/\text{h}$ ) to low ( $I = 1 \mu\text{M}/\text{h}$ ) production rates are explored. The parameter values for the four production levels considered are given in Table 1.

Cell geometry is as follows. The soma is  $10 \mu\text{m}$  in diameter and terminal segments are  $1 \mu\text{m}$  in diameter. Following a branching event, the new daughter terminal segments are given an initial length of  $5 \mu\text{m}$ , in keeping with experimental data indicating segments have a minimum length (van Pelt et al., 2001). The elongation rate of each terminal segment is  $0.22 \mu\text{m}/\text{h}$ , representing the average outgrowth resulting from periods of fast elongation and retraction for rat layer V pyramidal cell

Table 1  
Production and decay model parameter values that give an initial somatic concentration of  $1 \mu\text{M}$  for different production levels

$I(\mu\text{M}/\text{h})$	$\gamma_0(\text{h})$	$\gamma_T(\text{h})$
1000	990	100
10	9	100
2	1	100
1	0.01	100

basal dendrites (van Pelt and Uylings, 1999). Neurites are grown for 200 h with the terminal branching rate,  $k_b = 0.02/\mu\text{M h}$  (unless stated otherwise). Time interval  $dt$  is chosen to provide stable integration and ranges from  $10^{-3}$  to  $10^{-5}$  h. Statistics on the number of terminals (degree), centrifugal order of terminals and asymmetry of the tree were collected from 1000 simulated trees (100 trees for Purkinje cell simulations). Tree asymmetry is a measure of the relative difference in the number of terminals in the two subtrees at each bifurcation point. It is calculated as (van Pelt and Uylings, 1999):

$$A_l = \frac{1}{n-1} \sum_{j=1}^{n-1} \frac{|l_j - r_j|}{l_j + r_j - 2} \quad (6)$$

for  $l_j + r_j > 2$ , where  $n$  is the number of terminals in the tree and  $l_j$  and  $r_j$  are the number of terminals in the left and right subtrees at the  $j$ th bifurcation point.

For comparison with the *BESTL* model, *BESTL* model parameters were adjusted until tree distributions were obtained with the same mean and standard deviation for degree, centrifugal order and asymmetry. Appropriate sets of *BESTL* parameters could be found in all cases.

### 3. Results

#### 3.1. High production rate

Initially, we consider the form of neurite growth when production is high ( $I = 1000 \mu\text{M/h}$ ). In this situation the somatic concentration remains nearly constant at  $1 \mu\text{M}$  throughout the growth period.

Fig. 1(a) shows the equivalent *BESTL*  $E$  and  $S$  parameters that matched the *AD* model tree statistics obtained for different values of the branch power,  $e$ , that determines how segment diameters increase over time. Only active transport was included ( $a = 100 \mu\text{m/h}$ ,  $D = 0$ ). The *BESTL* branching rate  $B$  was 4 in all cases

(equal to the branch period multiplied by the *AD* branching rate:  $200 \times 0.02$ ). Clearly,  $E$  and  $S$  covaried with  $e$  and they are well matched by the relationship  $E = S = 1 - 2/e$ .

In these high production conditions with no diffusion, terminal concentrations are not limited by the availability of substance at the site of production in the cell body, but by how the substance is distributed by active transport. This is a function of segmental cross-sectional area. From the power law for segment diameters (Eq. (5)), it follows that, if all terminal segments have the same diameter,  $d_T$ , then

$$d_p = (d_l^e + d_r^e)^{1/e} = n_p^{1/e} d_T, \quad (7)$$

where  $n_p$  is the number of terminals in the subtree below segment  $p$ . In each time step, the relative amount of substance moved by active transport into each daughter segment is proportional to its relative cross-sectional area. For example, the proportion going into the left branch is:

$$\frac{A_l}{A_l + A_r} = \frac{d_l^2}{d_l^2 + d_r^2} = \frac{n_l^{2/e}}{n_l^{2/e} + n_r^{2/e}}. \quad (8)$$

In the *BESTL* model,  $S = 0$  indicates no dependence on centrifugal order. The same effect occurs here when  $e = 2$ , as the amount leaving a parent segment is split directly in proportion to the number of terminals in each subtree so that all terminals will receive the same amount of branch-determining substance. If  $e = \infty$  in the above equation, then the substance is split equally between the daughter branches, irrespective of the size of the individual subtrees. This has the same effect as  $S = 1$ , as then terminal branching probability decreases by a factor of 2 with each increment in centrifugal order. We can equate the two models by setting  $2/e = 1 - S$ .

Similarly, the amount of substance transported from the soma increases in proportion with the cross-sectional area of the initial segment,  $A_1$ :

$$A_1 \propto d_1^2 = n^{2/e} d_T, \quad (9)$$

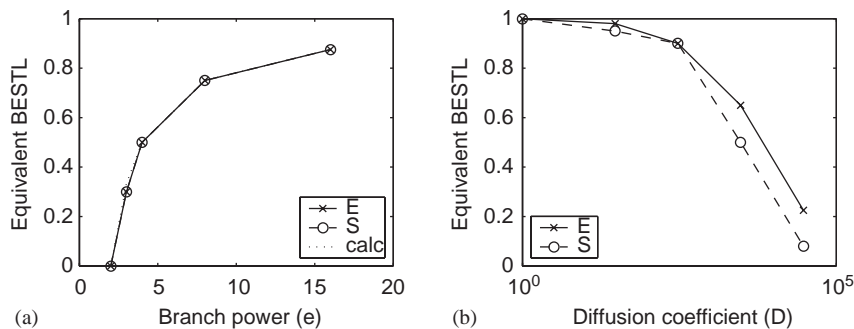


Fig. 1. Equivalent *BESTL* parameters  $E$  and  $S$  to match *AD* tree statistics in high production conditions ( $I = 1000 \mu\text{M/h}$ ). (a) Active transport ( $a = 100 \mu\text{m/h}$ ) and no diffusion ( $D = 0$ ), with branch power  $e$  varied (calc:  $E = S = 1 - 2/e$ ); (b) Active transport and fixed segment diameter, with diffusion coefficient varied from 0 to  $30,000 \mu\text{m}^2/\text{h}$ .

where  $n$  is the total number of terminals in the growing tree. Thus the *AD* and *BESTL* models can be equated by  $2/e = 1 - E$ .

Increasing diffusion rate, with fixed segment diameters, has a similar effect to decreasing the branch power (Fig. 1(b)). As more substance is transported by diffusion, concentrations throughout the tree become more uniform and so effects of the number of terminals and centrifugal order are reduced. For apparent physiological tubulin transport rates ( $a = 100 \mu\text{m}/\text{h}$ ,  $D = 30,000 \mu\text{m}^2/\text{h}$ ) terminal number and centrifugal order effects are small ( $E = 0.225$ ,  $S = 0.08$ ). With non-uniform segment diameters (small  $e$ ), equivalent  $E$  and  $S$  values are reduced further (results not shown), as in the case of no diffusion. For example, with  $a = 100 \mu\text{m}/\text{h}$ ,  $D = 30,000 \mu\text{m}^2/\text{h}$  and  $e = 4$ , the equivalent values are  $E = 0.08$ ,  $S = 0.02$ .

3.2. Lower production rates

If the production rate is sufficiently low, the somatic concentration is no longer constant but drops as new terminals are added to the growing tree and demand for the branch determining substance increases. This introduces a new factor that influences the equivalent  $E$  value, but not the  $S$  value, as shown in Fig. 2. For active transport only, the equivalent  $S$  value decreases with branch power  $e$  (increasing segment diameters), reaching zero when  $e = 2$ , and is independent of the

production rate (Fig. 2(b)). The situation for the equivalent  $E$  value is more complex (Fig. 2(a)). If segment diameter is uniform, then  $E = 1$  regardless of production rate. If segment diameters increase ( $e = 2$  or  $4$ ) over time, then  $E$  decreases with increasing production rate, becoming zero when  $I = 1000 \mu\text{M}/\text{h}$  and  $e = 2$ . Here,  $E$  remains high at low production levels due to reduction in the soma concentration as more substance is transported from the soma as diameters increase. Thus the increased transport is nullified by a lack of resource. The same situation arises for increasing diffusion rates, with uniform segment diameters (Fig. 2(c), (d)). Now, increased transport due to faster diffusion is nullified by a lack of resource in low production conditions. As this affects the amount of substance available to all terminals, the centrifugal order effect ( $S$  value) is not altered.

Thus changes in production rate alter the effects due to the number of terminals but not their centrifugal order, introducing some independence in the equivalent  $E$  and  $S$  values. Such independence is apparent in the statistics from real dendritic trees, as will be explored below.

3.3. Effect of decay or consumption at a terminal

Varying the terminal consumption/decay rate  $\gamma_T$  has different effects depending on whether active transport or diffusion is the dominant transport mechanism.

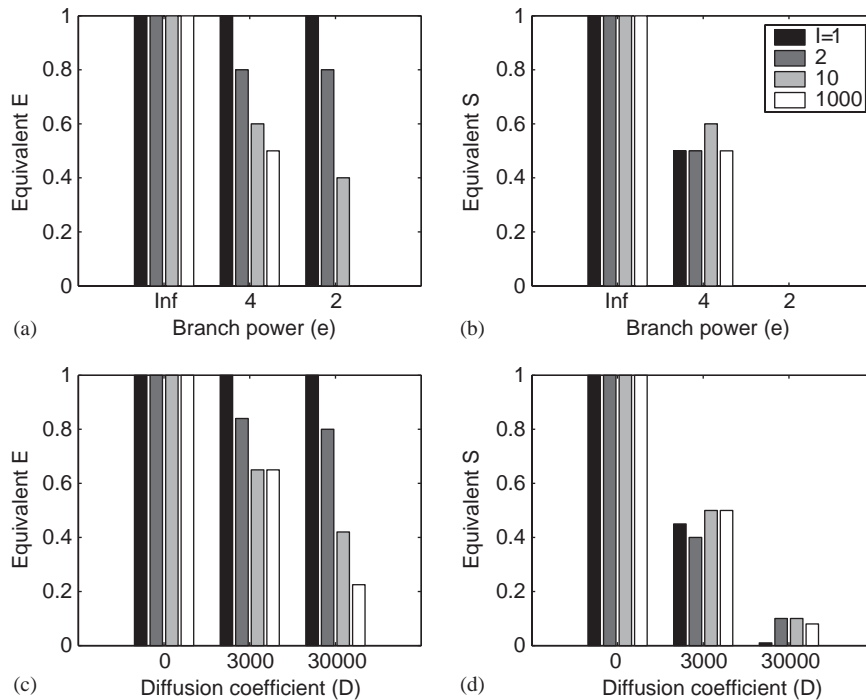


Fig. 2. Equivalent *BESTL* parameters to match *AD* tree statistics in varying production conditions. (a), (b) Active transport ( $a = 100 \mu\text{m}/\text{h}$ ) and no diffusion ( $D = 0$ ), with branch power  $e$  varied (Inf is uniform diameter); (c), (d) Active transport and fixed segment diameter, with diffusion coefficient varied. Missing bars correspond to zero values.

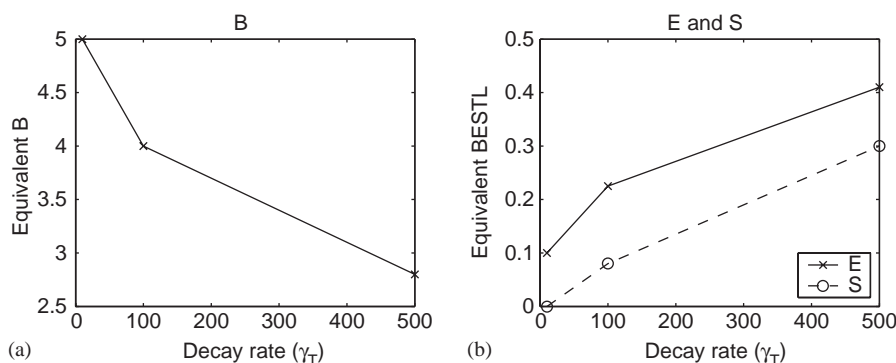


Fig. 3. Equivalent *BESTL* parameter values when terminal consumption/decay rate  $\gamma_T$  is varied.  $a = 100 \mu\text{m}/\text{h}$ ,  $D = 30000 \mu\text{m}^2/\text{h}$ ,  $I = 1000 \mu\text{M}/\text{h}$ ,  $\gamma_0 = 990/\text{h}$  and uniform diameter throughout.

Without diffusion,  $\gamma_T$  acts simply to set the base branching rate (equivalent *B* value). Increasing  $\gamma_T$  decreases the equivalent *B* value, and vice versa (e.g.  $\gamma_T = 50/\text{h}$  gives  $B = 8$ ;  $\gamma_T = 200/\text{h}$  gives  $B = 2$ ). When diffusion is dominant, the effect on the base branching rate is reduced and variations in the equivalent *E* and *S* values are introduced, due to the equilibrating effect of diffusion on concentration levels throughout the tree. For example, raising  $\gamma_T$  decreases the equivalent *B* value whilst increasing the equivalent *E* and *S* values as the increased consumption affects the entire tree when new terminals are added. Example equivalent *BESTL* parameter values are given in Fig. 3 for variations in  $\gamma_T$ .

### 3.4. Matching statistics of real dendritic trees

The *BESTL* model is able to well fit topological tree statistics from a range of different neuronal tree types (van Pelt et al., 1997, 2001, 2003; van Pelt and Uylings, 1999). Though the complete real neuronal data is not published, we can explore the ability of the *AD* model to produce different tree types by comparing it with *BESTL* model output using the optimal *BESTL* parameter values found for particular neuronal trees (van Pelt et al., 1997, 2001, 2003; van Pelt and Uylings, 1999). The *AD* model was fit by trial-and-error to *BESTL* degree, centrifugal order and asymmetry distributions by varying production rate  $I$  and branch power  $e$  with only active transport ( $a = 100 \mu\text{m}/\text{h}$ ,  $D = 0$ ). The match between the *BESTL* and *AD* distributions for four different dendritic tree types is shown in Fig. 4. There is a strong similarity between most of the distributions, as revealed by chi-square test  $p$ -values. In particular, the match between the degree distributions is of the same order as the match between the *BESTL* model and the distributions from real trees, as reported in van Pelt et al. (1997). The optimal *BESTL* (taken from the literature cited above) and corresponding *AD* parameter values are given in Table 2.

Clearly, the variety of dendritic tree topologies found in real neurons is able to be reproduced by the *AD* model through variations in production and transport of the branch-determining substance. Note that all the tree types are best matched by the *AD* model in low production conditions during which a reduction in the soma concentration contributes to a reduction in branching probability with the increase in the number of terminals in the tree. Both the base branching rate  $k_{br}$  and the branch power  $e$  vary with tree type. The increase in branching probability with centrifugal order apparent for Purkinje cells (negative *S* value) is achieved with a branch power  $e$  less than 2, so that proportionally more substance is transported into larger subtrees.

## 4. Discussion

The *BESTL* model of neurite outgrowth indicates that branching is affected by the number of terminals in the growing tree and their centrifugal orders. It is not clear how such dependencies might arise in the real neuron. Here we have investigated a model in which branching depends on the amount of a substance in each dendritic terminal. The substance is produced in the cell body and must be transported to the terminals, where it promotes branching. The interaction of production and transport introduces similar branching dependencies to those exhibited by the *BESTL* model.

### 4.1. Effects due to active transport

When active transport is the dominant mechanism, branching effects due to the number of terminals in the growing tree and their centrifugal order arise due to how the transport mechanism distributes the branch-determining substance throughout the tree. In our model it is assumed that the rate of active transport is proportional to the cross-sectional area of a tree segment. This is on the basis that an increase in segment diameter includes

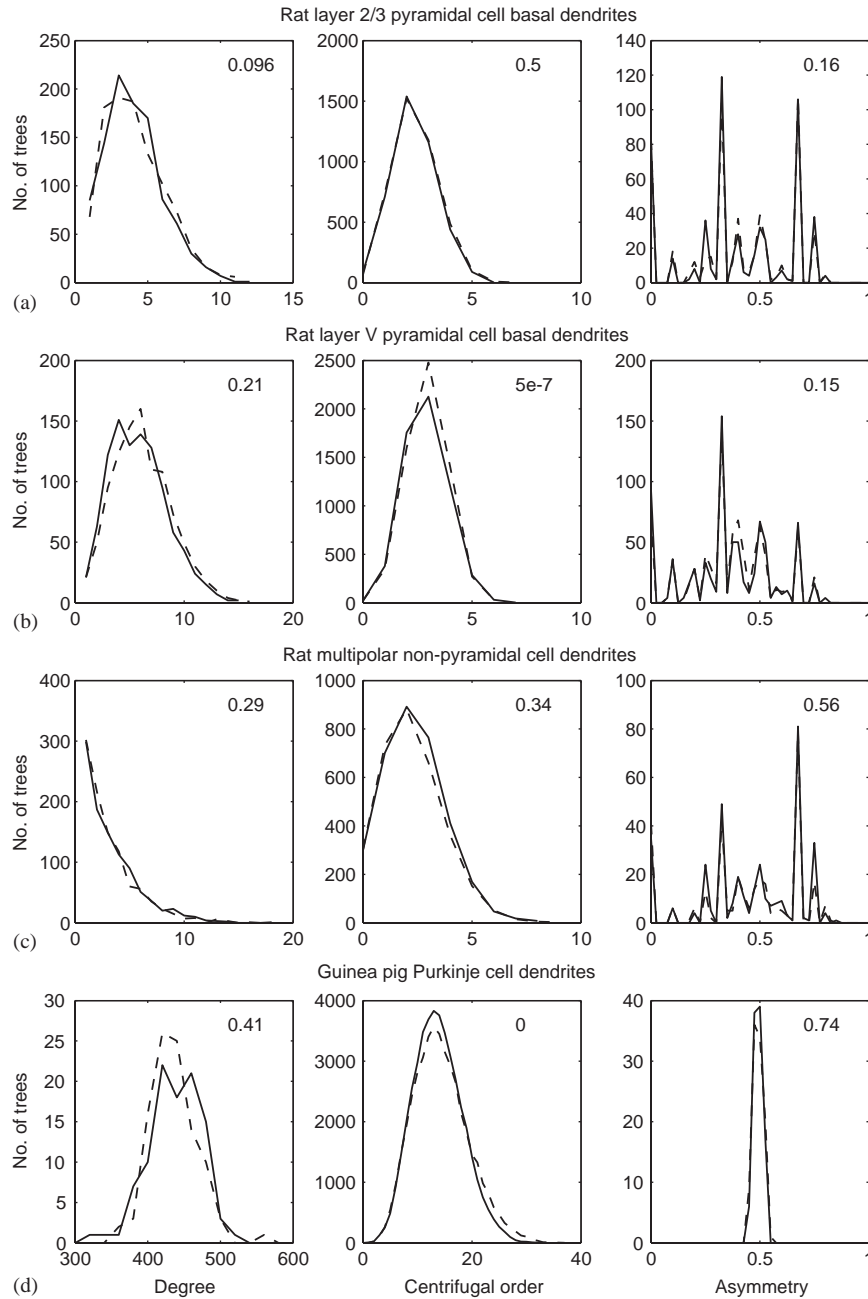


Fig. 4. (a–d) Match of *AD* model to *BESTL* model optimized to the tree statistics from different neuronal types (see Table 2 for details of tree types). Solid lines: *AD*; dashed lines: *BESTL*. Data from 1000 simulated trees; except 100 trees only for Purkinje cells. Numbers on each graph are chi-square test *p*-values, indicating the similarity of the distributions.

Table 2  
*BESTL* and *AD* parameter values required to match real tree statistics

Tree	$B$	$E$	$S$	$k_{br}/(\mu\text{M h})$	$e$	$I(\mu\text{M/h})$	$\gamma_0(\text{/h})$	$\gamma_r(\text{/h})$
PC 2/3	2.52	0.73	0.5	0.0126	4	2	1	100
PC 5	3.85	0.74	0.87	0.01925	8	10	9	100
non-PC	1.26	0.106	0	0.0063	2	20	19	100
Purkinje	95	0.69	-0.14	0.13	1.7	20	19	100

PC 2/3 are rat cortical layer 2/3 pyramidal cell basal dendrites (van Pelt et al., 2001); PC 5 are rat cortical layer V pyramidal cell basal dendrites (van Pelt and Uylings, 1999); non-PC are rat cortical layer IV multipolar non-pyramidal cell dendrites (van Pelt et al., 2003); Purkinje are guinea pig Purkinje cell dendrites (van Pelt et al., 2001).

an increase in the number of microtubules and consequently an increase in the molecular machinery providing active transport.

A strong centrifugal order effect arises if daughter branches have very similar diameters to the parent branch, irrespective of the size of the subtrees (large  $e$ ). The *BESTL* model that best fits the growth of the basal dendrites of large layer V neocortical pyramidal cells has a value of  $S = 0.87$  (van Pelt and Uylings, 1999). This corresponds to  $e \approx 16$ . The physical diameters of real dendrites are generally approximated by  $1 \leq e \leq 2$  (van Pelt and Uylings, 1999). That is, real dendrites show much greater variation in dendritic diameters than this dependence on centrifugal order implies. It is possible that the amount of substance transported into a segment increases only marginally with an increase in physical cross-sectional area, rather than in direct proportion. This is in accord with the decrease in microtubule density seen with increasing neurite diameter (Alvarez et al., 2000). In contrast, other tree types do not display such a strong dependence on centrifugal order, inline with the model of increasing transport with increasing segment diameters (see Table 2). So the *AD* model depends on a power law setting of transport area in each new branch, but this may be different from that which describes the anatomical diameters of different branches.

In the *AD* model, with high production and no diffusion, the branch power  $e$  effectively sets both the equivalent *BESTL* parameters according to the relationship  $E = S = 1 - 2/e$ . Previously we defined a steady-state model in which the production of the substance in the cell body is regulated by the number of terminals in the tree and the substance is distributed throughout the tree according to the relative sizes of subtrees (Graham et al., 1998; van Pelt et al., 2003). It differs from the *AD* model in that no transport mechanism is specified and, importantly, effects due to the number of terminals ( $E$ ) and their centrifugal order ( $S$ ) are independent. This model behaves identically to the *BESTL* model for the same values of the  $E$  and  $S$  parameters (van Pelt et al., 2003). The *AD* model provides a possible implementation of this based on active transport, with the limitation that  $E = S$ . Some independence between  $E$  and  $S$  arises in the *AD* model when production rates are low or diffusion accounts for a proportion of the transport.

#### 4.2. Effects due to diffusion

The effect of diffusion is to equilibrate, to some extent, the substance concentration throughout the growing tree. The physiological rate of diffusion for oligomeric tubulin in axoplasm ( $D = 30000 \mu\text{m}^2/\text{h}$ ) results in low equivalent values of  $E$  and  $S$  in high production conditions (Fig. 1(b)). That is, the effects of the number of terminals and centrifugal order on

branching are small. Terminal number and centrifugal order effects become much stronger at diffusion rates an order of magnitude lower than this, as might apply for transport of polymerized proteins (Galbraith et al., 1999). For  $D \leq 300 \mu\text{m}^2/\text{h}$  the equivalent  $E$  and  $S$  values are close to 1, irrespective of the production rate. At high diffusion rates, the effect of centrifugal order remains small, independent of variations in production rate (Fig. 2(d)). The effect of the number of terminals, however, is now strongly dependent on the production rate (Fig. 2(c)). When production is low, diffusion is very successful at equilibrating concentration throughout the cell, including the soma. Consequently, the addition of new terminals introduces extra consumption ( $\gamma_T$ ) which lowers concentration levels in proportion to the number of terminals in the tree. So now an equivalent  $E$  effect arises from consumption of the branch-determining substance at the terminals, rather than through distribution of a finite amount of substance to all terminals, as in the active transport-dominant case.

In conditions in which equilibration is achieved (low production and small soma volume with high diffusion) the soma and terminal concentrations are given by (derivation in Appendix A):

$$C_0 \approx C_T \approx \frac{I}{\gamma_0 + n\gamma_T}, \quad (10)$$

where  $n$  is the total number of terminals in the tree. This dependency of terminal concentration on the total number of terminals in the tree is similar to the  $E$  effect in the *BESTL* model. Appropriate values of  $\gamma_0$  and  $\gamma_T$  can be chosen to approximate the effect of a given value of  $E$ , as illustrated in Fig. 5.

For the cell used here this dependency does not strictly hold as the large size of the soma provides a sufficient reservoir of substance that diffusion cannot equilibrate the entire cell, even at low production rates.

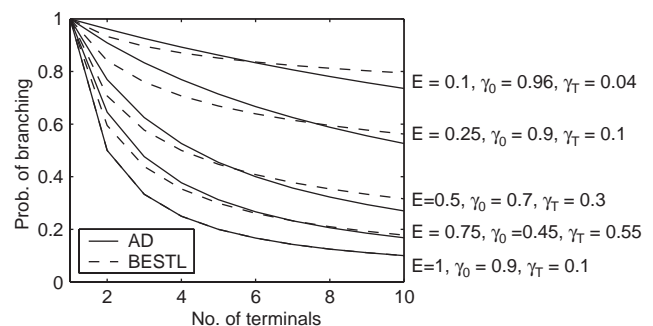


Fig. 5. Dependency of the probability of branching on the number of terminals in a growing tree for the *BESTL* and diffusion dominant *AD* models. Values for  $\gamma_0$  and  $\gamma_T$  to approximate the *BESTL* terminal number dependency  $E$  are given to the right of each trace. The production rate is  $I = 1$ .

Thus  $E$  and  $S$  effects due to transport limitations are still present (see Fig. 3).

#### 4.3. Branching rate over time

During neurite development it is highly likely that the base branching rate ( $B$  parameter in the *BESTL* model) is not constant over time. Data from rat multipolar non-pyramidal cells indicate that the base branching rate decays exponentially with time, irrespective of terminal number and centrifugal order effects (van Pelt and Uylings, 2002). The *AD* model displays an effective constant base branching rate with time. Thus the transport-limited effects demonstrated here do not include a reduction in branching rate over time. Production rate  $I$  has been assumed constant in the *AD* model, but a reduction in branching rate would arise if production declined with time.

### 5. Conclusions

A model of dendritic branching in which a terminal's branching rate is determined by the concentration of a substance, such as tubulin, is introduced. This model demonstrates how branching dependencies on the number of terminals and their centrifugal order, as described by the *BESTL* model (van Pelt and Uylings, 1999), may arise due to the active transport and diffusion of the branch-determining substance. When active transport is dominant, the dependencies arise through increases in the available transport area as tree segment diameters increase as a function of the size of their supported subtrees. This model is sufficient to match the tree statistics from a variety of real neuronal dendrites. If diffusion is dominant, the effects of substance consumption in each terminal are transmitted throughout the tree by the equilibrating effect of diffusion. This introduces dependencies on the number of terminals and their centrifugal order that are determined by the substance production and decay rates.

Experiments that measure the transport and concentration of branch-determining substances such as tubulin and MAPs along growing neurites would help verify our model. From the comparison with real trees (Fig. 4 and Table 2), our model predicts that the concentration of the substance, for example tubulin, will decrease throughout the tree as the tree grows and branches. This will be most marked in those tree types that exhibit a strong modulation in branching as the tree becomes more branched (high equivalent  $E$  value), as in pyramidal cell basal dendrites. These trees should also have a relatively low substance production rate. Those tree types that show modulation in branching with centrifugal order will exhibit variability in the substance

concentration at terminal growth cones. Where branching decreases with centrifugal order, again as in pyramidal cell basal dendrites, the growth cones of larger subtrees will have a lower concentration than those of smaller (less branched) subtrees. For Purkinje cells the opposite should be the case. There larger subtrees will show a higher growth cone concentration. The relative concentrations in two daughter branches immediately following a branch point should also be indicative of centrifugal order effects. Here, similar concentrations in the daughter branches should correlate with a strong centrifugal order effect. A higher concentration in the daughter branch of the larger subtree should correlate with limited modulation in branching with centrifugal order.

Experiments that disrupt active transport mechanisms would clarify the relative contributions of active transport and diffusion to the growth process. This would require specific interruption to the active transport of say, tubulin, without altering the active transport of other organelles. If this was possible then, if active transport is the dominant mechanism, tree growth would be severely stunted. If active transport and diffusion both contribute, then apart from some loss in branching due to the removal of one transport mechanism, a reduction in any centrifugal order effects should also be evident when only fast diffusion is available for transport. Concentration gradients throughout the tree should also become more uniform.

This *AD* model is very simple both in its description of the biological processes involved in neurite outgrowth and branching, and in its numerical implementation. In ongoing work we are developing both more detailed and necessarily complex models (Hely, 2001), and numerically accurate techniques for simulating the growth of neurites in space and time (Graham and van Ooyen, 2001; McLean et al., 2003). A more complete description of neuronal growth will include the generation of dendrites in 3D space, with appropriate formation of branching angles (Tamori, 1993), and the pathfinding of terminal growth cones through the external environment (Li et al., 1995; van Veen and van Pelt, 1992).

#### Acknowledgements

This work was funded in part by EPSRC grant GR/R89769/01 to BPG.

#### Appendix A. Simplification of diffusion-only model

An appreciation of the behaviour of a diffusion dominant model can be gained by considering the terminal concentrations when  $n$  branches are all growing from the soma. The changes in concentration over time

in the cell body and at the terminals are given by

$$\frac{dC_0}{dt} = I - \gamma_0 C_0 + \sum_{i=1}^n \frac{DA_T}{L_T V_0} (C_T - C_0), \quad (\text{A.1})$$

$$\frac{dC_T}{dt} = -\gamma_T C_T + \frac{DA_T}{L_T V_T} (C_0 - C_T), \quad (\text{A.2})$$

where  $L_T$  is the intracellular longitudinal distance between terminal  $T$  and the cell body,  $A_T$  is the available cross-sectional area (assumed uniform along the length of the branch) and  $V_T$  is the volume into which diffusion takes place.

In the steady-state the cell body and terminal concentrations can be calculated explicitly. We assume that all terminals are equidistant from the root, with distance  $L$ , and have equal decay rates,  $\gamma_T$ , and all branches have the same cross-sectional area,  $A$ . All terminal concentrations will then be the same and thus:

$$\frac{dC_0}{dt} = I - \gamma_0 C_0 + \frac{nDA}{LV_0} (C_T - C_0) = 0, \quad (\text{A.3})$$

$$\Rightarrow I + \frac{nDA}{LV_0} C_T = \left( \gamma_0 + \frac{nDA}{LV_0} \right) C_0, \quad (\text{A.4})$$

$$\Rightarrow C_0 = \frac{LV_0 I + nDAC_T}{\gamma_0 LV_0 + nDA}. \quad (\text{A.5})$$

Substituting this expression for  $C_0$  into the equation for  $C_T$  gives

$$\frac{dC_T}{dt} = -\gamma_T C_T + \frac{DA}{LV_T} \left( \frac{LV_0 I + nDAC_T}{\gamma_0 LV_0 + nDA} - C_T \right) = 0, \quad (\text{A.6})$$

$$\Rightarrow \left( \frac{DA}{LV_T} + \gamma_T - \frac{nD^2 A^2}{LV_T (\gamma_0 LV_0 + nDA)} \right) C_T = \frac{DIAV_0}{(\gamma_0 LV_0 + nDA)V_T}, \quad (\text{A.7})$$

$$\Rightarrow C_T = \frac{DIAV_0}{\gamma_0 \gamma_T LV_0 V_T + (\gamma_0 V_0 + n\gamma_T V_T) DA}. \quad (\text{A.8})$$

If diffusion is fast so that  $DA$  is large, and  $V_0 \approx V_T$  then the above reduces to

$$C_0 \approx C_T \approx \frac{I}{\gamma_0 + n\gamma_T}. \quad (\text{A.9})$$

## References

Acebes, A., Ferrus, A., 2000. Cellular and molecular features of axon collaterals and dendrites. *TINS* 23, 557–565.  
 Alvarez, J., Giuditta, A., Koenig, E., 2000. Protein synthesis in axons and terminals: significance for maintenance, plasticity and regulation of phenotype; with a critique of slow transport theory. *Prog. Neurobiol.* 62, 1–62.

Audesirk, G., Cabell, L., Kern, M., 1997. Modulation of neurite branching by protein phosphorylation in cultured rat hippocampal neurons. *Dev. Brain Res.* 102, 247–260.  
 Burke, R., Marks, W., Ulfhake, B., 1992. A parsimonious description of motoneuron dendritic morphology using computer simulation. *J. Neurosci.* 12, 2403–2416.  
 Carriquiry, A., Ireland, W., Kliemann, W., Uemura, E., 1991. Statistical evaluation of dendritic growth models. *Bull. Math. Biol.* 53, 579–589.  
 Cline, H., 2001. Dendritic arbor development and synaptogenesis. *Curr. Opin. Neurobiol.* 11, 118–126.  
 Dityatev, A., Chmykhova, N., Studer, L., Karamian, O., Kozhanov, V., Clamann, H., 1995. Comparison of the topology and growth rules of motoneuronal dendrites. *J. Comp. Neurol.* 363, 505–516.  
 Galbraith, J., Reese, T., Schlieff, M., Gallant, P., 1999. Slow transport of unpolymerized tubulin and polymerized neurofilament in the squid giant axon. *Proc. Natl Acad. Sci.* 96, 11589–11594.  
 Graham, B., Hely, T., vanOoyen, A., 1998. An internal signalling model of the dendritic branching process. *Euro. J. Neurosci.* 10 (Suppl. 10), 274.  
 Graham, B., van Ooyen, A., 2001. Compartmental models of growing neurites. *Neurocomputing* 38–40, 31–36.  
 Hely, T., 2001. A computational model of dendrite elongation and branching based on MAP2 phosphorylation. *J. Theor. Biol.* 210, 375–384.  
 Hillman, D., 1979. Neuronal shape parameters and substructures as a basis of neuronal form. In: Schmitt, F., Worden, F. (Eds.), *The Neurosciences, Fourth Study Program*. MIT Press, Cambridge, MA, pp. 477–498.  
 Kobayashi, N., Mundel, P., 1998. A role of microtubules during the formation of cell processes in neuronal and non-neuronal cells. *Cell Tissue Res.* 291, 163–174.  
 Li, G.-H., Qin, C.-D., Wang, L.-W., 1995. Computer model of growth cone behavior and neuronal morphogenesis. *J. Theor. Biol.* 174, 381–389.  
 Maccioni, R., Cambiazo, V., 1995. Role of microtubule-associated proteins in the control of microtubule assembly. *Physiol. Rev.* 75, 835–857.  
 McLean, D., van Ooyen, A., Graham, B., 2003. Continuum model for tubulin-driven neurite elongation. In: *Computational Neuroscience*. July, Alicante, Spain  
 Miller, K., Samuels, D., 1997. The axon as a metabolic compartment: protein degradation, transport and maximum length of an axon. *J. Theor. Biol.* 186, 373–379.  
 Mitchison, T., Kirschner, M., 1984. Dynamic instability of microtubule growth. *Nature* 312, 237–242.  
 Nowakowski, R., Hayes, N., Egger, M., 1992. Competitive interactions during dendritic growth: a simple stochastic growth algorithm. *Brain Res.* 576, 152–156.  
 Odde, D., 1997. Estimation of the diffusion-limited rate of microtubule assembly. *Biophys. J.* 73, 88–96.  
 Rall, W., 1959. Branching dendritic trees and motoneuron membrane resistivity. *Exp. Neurol.* 1, 491–527.  
 Redmond, L., Ghosh, A., 2001. The role of Notch and Rho GTPase signalling in the control of dendritic development. *Curr. Opin. Neurobiol.* 11, 111–117.  
 Shah, J., Cleveland, D., 2002. Slow axonal transport: fast motors in the slow lane. *Curr. Opin. Cell Biol.* 14, 58–62.  
 Tamori, Y., 1993. Theory of dendritic morphology. *Phys. Rev. E* 48, 3124–3129.  
 Uemura, E., Carriquiry, A., Kliemann, W., Goodwin, J., 1995. Mathematical modeling of dendritic growth in vitro. *Brain Res.* 671, 187–194.  
 van Pelt, J., Uylings, H., 1999. Natural variability in the geometry of dendritic branching patterns. In: Pozanski, R. (Ed.), *Modeling in*

- the Neurosciences: From Ionic Channels to Neural Networks. Harwood Academic, pp. 79–108 (Chapter 4).
- van Pelt, J., Uylings, H., 2002. Branching rates and growth functions in the outgrowth of dendritic branching patterns. *Network* 13, 261–281.
- van Pelt, J., Dityatev, A., Uylings, H., 1997. Natural variability in the number of dendritic segments: model-based inferences about branching during neurite outgrowth. *J. Comp. Neurol.* 387, 325–340.
- van Pelt, J., van Ooyen, A., Uylings, H., 2001. Modeling dendritic geometry and the development of nerve connections. In: De Schutter, E. (Ed.), *Computational Neuroscience: Realistic Modeling for Experimentalists*. CRC Press, Boca Raton, FL, pp. 179–208 (Chapter 7).
- van Pelt, J., Graham, B., Uylings, H., 2003. Formation of dendritic branching patterns. In: van Ooyen, A. (Ed.), *Modeling Neural Development*. MIT Press, Cambridge, MA, pp. 75–94 (Chapter 4).
- van Veen, M., van Pelt, J., 1992. A model for outgrowth of branching neurites. *J. Theor. Biol.* 159, 1–23.
- Whitford, K., Dijkhuizen, P., Polleux, F., Ghosh, A., 2002. Molecular control of cortical dendrite development. *Ann. Rev. Neurosci.* 25, 127–149.